

## ORIGINAL ARTICLE

# Short-term prediction of UT1-UTC and LOD via Dynamic Mode Decomposition and combination of least-squares and vector autoregressive model

Maciej Michalczak<sup>1\*</sup> and Marcin Ligas<sup>1</sup><sup>1</sup>Department of Integrated Geodesy and Cartography, Faculty of Geo-Data Science, Geodesy, and Environmental Engineering, AGH University of Krakow, al. Adama Mickiewicza 30, 30-059 Kraków

\*mmichalc@agh.edu.pl

## Abstract

This study presents a short-term forecast of UT1-UTC and LOD using two methods, i.e. Dynamic Mode Decomposition (DMD) and combination of Least-Squares and Vector Autoregression (LS+VAR). The prediction experiments were performed separately for yearly time spans, 2018–2022. The prediction procedure started on January 1 and ended on December 31, with 7-day shifts between subsequent 30-day forecasts. Atmospheric Angular Momentum data (AAM) were used as an auxiliary time series to potentially improve the prediction accuracy of UT1-UTC and LOD in LS+VAR procedure. An experiment was also conducted with and without elimination of effect of zonal tides from UT1-UTC and LOD time series. Two approaches to using the best steering parameters for the methods were applied: First, an adaptive approach, which observes the rule that before every single forecast, a preliminary one must be performed on the pre-selected sets of parameters, and the one with the smallest prediction error is then used for the final prediction; and second, an averaged approach, whereby several forecasts are made with different sets of parameters (the same parameters as in adaptive approach) and the final values are calculated as the averages of these predictions. Depending on the method and data combination mean absolute prediction errors (MAPE) for UT1-UTC vary from 0.63 ms to 1.43ms for the 10th day and from 3.07 ms to 8.05ms for the 30th day of the forecast. Corresponding values for LOD vary from 0.110 ms to 0.245 ms for the 10th day and from 0.148 ms to 0.325 ms for the 30th day.

**Key words:** UT1-UTC, length of day, dynamic mode decomposition, autoregression, prediction

## 1 Introduction

The Earth Orientation Parameters (EOP) describe the irregularities of the Earth's rotation and its orientation in space. They include three classes of parameters, i.e. Earth pole coordinates (PMx and PMy), the difference between Universal Time (UT1) and Universal Coordinated Time (UTC), determined by atomic clocks, i.e. UT1-UTC and Celestial Pole Offsets (dX and dY, yielded by the precession-nutation models). This set of parameters is essential to perform the conversion between Celestial Reference Frame (CRF) and Terrestrial Reference Frame (TRF) (Gambis and Luzum, 2011). Knowledge of EOP plays a significant role in several other astronomical and geodetic applications, including: space navigation, precise

orbit determination, and climate forecasting and analysis.

The Length of a Day (LOD) is the first negative derivative from the UT1-UTC after removing leap seconds and is determined as the difference between the astronomically determined duration of the Earth's rotation and 86400 SI seconds. Both parameters are used to model changes in the Earth's rotation rate (Modiri et al., 2020). The following factors play an important role in the variability of UT1-UTC and LOD, e.g.: El Niño Southern Oscillation (Holton and Dmowska, 1989; Soffel, 2013), zonal wind variations in atmospheric general circulation models (Höpfner, 1998), and ice mass loss and the resulting sea level changes (Gross et al., 2004). According to Xu et al. (2022b) LOD is also strongly related to The El Niño-Southern Oscillation (ENSO) and Atmospheric Angular Momentum (AAM)

changes, across the frequencies of interannual oscillations.

Determination of EOP with a high accuracy combines such advanced geodetic techniques as Very Long Baseline Interferometry (VLBI), Global Navigation Satellite System (GNSS), Satellite Laser Ranging (SLR), Lunar Laser Ranging (LLR), and Doppler Orbitography and Radiopositioning Integrated by Satellite (DORIS). This combination enables a determination of EOP with accuracy of approximately 50  $\mu$ s or higher in the case of pole coordinates and 30  $\mu$ s or higher in the case of UT1-UTC (10  $\mu$ s for LOD) (Dick and Thaller, 2020).

The final EOP data are usually provided with delay caused by the complexity of measuring and data processing, and published, for example, by the International Earth Rotation and Reference Systems Service (IERS) after 30 days (Dick and Thaller, 2020). This latency gap can be filled using rapid products (published by, e.g., IERS (Daily Rapid EOP Data), CODE (Center for Orbit Determination in Europe), GFZ (German Research Centre for Geosciences), or IGS (International GNSS Service)). For several astronomical and geodetic purposes, the knowledge of the near real-time EOP data is needed. The solution to this problem is EOP prediction.

EOP prediction is commonly used, as evidenced by two comparison campaigns, organised by IERS, i.e., the 1st Earth Orientation Parameters Prediction Comparison Campaign held in 2006–2008 (Kalarus et al., 2010) and the 2nd Earth Orientation Parameters Prediction Comparison Campaign held in 2021–2022 (<http://eoppcc.cbk.waw.pl>, Kur et al. 2022; Śliwińska et al. 2022). Also, within a GGOS (Global Geodetic Observing System) infrastructure, a Joint Study Group 3: AI for Earth Orientation Parameter Prediction has been established (<https://ggos.org/about/org/fa/ai-for-geodesy/eop-prediction/>).

A number of techniques and data combinations have been used and developed to improve the accuracy of EOP prediction, e.g., neural networks (Guessoum et al., 2022; Liao et al., 2012; Schuh et al., 2002), machine learning (Kiani Shahvandi et al., 2022; Lei et al., 2017), kriging (Michalczak and Ligas, 2021, 2022), kalman filter (Gross et al., 1998; Nastula et al., 2020; Xu et al., 2012), singular spectrum analysis (Okhotnikov and Golyandina, 2019), or autoregressive models (Dill et al., 2018; Niedzielski and Kosek, 2011).

In this contribution, to predict UT1-UTC and LOD, the methods of Dynamic Mode Decomposition (DMD) and combination of least-squares and vector autoregression (LS+VAR) were used. DMD is a data-driven, equation-free technique capable of reconstructing and forecasting time series in a single numerical procedure whilst VAR is a multivariate counterpart of the Autoregressive (AR) model. DMD was applied to the separate UT1-UTC and LOD prediction whilst LS+VAR model was fed with UT1-UTC, LOD and Atmospheric Angular Momentum (AAM) series in various combinations (all used data combinations are explained in Table 1). AAM information, as an auxiliary variable, was applied to potentially strengthen the prediction of UT1-UTC and LOD in the LS+VAR model. The study also examined the difference in the accuracy of prediction with and without removing the effect of zonal tides.

This study attempts to answer the question of whether the direct incorporation of additional external data (Liouville equation not involved), such as AAM motion term, can improve LS+VAR predictions of UT1-UTC and LOD. This study also examines the impact of the removal of the effect of zonal tides from the UT1-UTC and LOD time series.

## 2 Prediction methods

### 2.1 Dynamic Mode Decomposition

DMD, based on fluid dynamics (Schmid, 2010), is a data-driven method of reconstructing and forecasting generally non-linear dynamical systems using linear techniques. It is governed by a main relation that links future states of a system to past ones through

an (unknown) operator  $\mathbf{A}$  that stores the dynamics of the system's evolution:

$$\mathbf{x}_{k+1} = \mathbf{A}\mathbf{x}_k \quad (1)$$

where  $\mathbf{x}_k$  and  $\mathbf{x}_{k+1}$  are the subsequent snapshots (images of a dynamical system) at discrete time instances  $t_k$  and  $t_{k+1}$ .

This equation has the form of a linear homogeneous system of difference equations with constant coefficients with some initial vector  $\mathbf{x}_1$  which is known to have the solution given by:

$$\mathbf{x}_{k+1} = \mathbf{A}^k \mathbf{x}_1 = \Phi \Lambda^k \Phi^{-1} \mathbf{x}_1 \quad (2)$$

where  $\Phi \Lambda \Phi^{-1}$  is the eigendecomposition of  $\mathbf{A}$ .

DMD algorithm searches the best-fit matrix  $\mathbf{A}$  in (1) (in fact its dominant eigenstructure). This is accomplished by generating a snapshot matrix  $\mathbf{X} = [\mathbf{x}_1, \mathbf{x}_2, \mathbf{x}_3, \dots, \mathbf{x}_m]$  that stores states of a system at discrete time instances  $t = 1, 2, \dots, m$ . The matrix is split into two other matrices,  $\mathbf{X}_1 = [\mathbf{x}_1, \mathbf{x}_2, \dots, \mathbf{x}_{m-1}]$  and  $\mathbf{X}_2 = [\mathbf{x}_2, \mathbf{x}_3, \dots, \mathbf{x}_m]$ , that are related, according to (1), by a matrix  $\mathbf{A}$ , i.e.:

$$\mathbf{X}_2 = \mathbf{A}\mathbf{X}_1 \quad (3)$$

The estimate of an operator  $\mathbf{A}$  is given by:

$$\mathbf{A} = \mathbf{X}_2 \mathbf{X}_1^+ \quad (4)$$

where  $\mathbf{X}_1^+ = \mathbf{V}\Sigma^{-1}\mathbf{U}^T$  denotes the Moore–Penrose pseudo-inverse determined using the singular value decomposition (SVD). This enables for a low dimensional representation of  $\mathbf{A}$  (Tu et al., 2014) by:

$$\tilde{\mathbf{A}} = \mathbf{U}^T \mathbf{A} \mathbf{U} = \mathbf{U}^T \mathbf{X}_2 \mathbf{V} \Sigma^{-1} \quad (5)$$

Eigenvalues of  $\tilde{\mathbf{A}}$  are those of  $\mathbf{A}$  and are obtained as a solution to the eigenvalue problem:

$$\tilde{\mathbf{A}}\mathbf{W} = \mathbf{W}\Lambda \quad (6)$$

whilst the eigenvectors of  $\mathbf{A}$  are given by:

$$\Phi = \mathbf{X}_2 \mathbf{V} \Sigma^{-1} \mathbf{W} \quad (7)$$

For high dimensional problems SVD of  $\mathbf{X}_1$  in (4) is truncated to some prescribed rank  $r$  (low rank approximation of  $\mathbf{X}_1$ ) yielding:

$$\mathbf{X}_1 \approx \mathbf{U}_r \Sigma_r \mathbf{V}_r^T \quad (8)$$

With this approximation, the algorithm works identically as previously with components of decomposition  $\mathbf{U}$ ,  $\Sigma$ ,  $\mathbf{V}$  replaced with  $\mathbf{U}_r$ ,  $\Sigma_r$ ,  $\mathbf{V}_r$ . Once the eigenstructure of  $\mathbf{A}$  is determined, (2) can be used to reconstruct or predict future states of the system. For low dimensional problems (numerically tractable) operator  $\mathbf{A}$  may be obtained from (4) and applied directly to (1).

In the case of time series analysis, the snapshot matrix becomes a trajectory matrix (known from, e.g., singular spectrum analysis), as described by Tirunagari et al. (2017). Hence, the input time series  $\mathbf{x}$  of length  $T$  is split into  $L$  subseries  $\mathbf{x}'$  of length  $K$  that are moved by one time step ahead, i.e.:

$$\mathbf{X} = \begin{bmatrix} x_1 & x_2 & \cdots & x_L \\ x_2 & x_3 & \cdots & x_{L+1} \\ \vdots & \vdots & \ddots & \vdots \\ x_K & x_{K+1} & \cdots & x_{K+L-1} \end{bmatrix} = [\mathbf{x}'_1 \quad \mathbf{x}'_2 \quad \cdots \quad \mathbf{x}'_L] \quad (9)$$

where  $L$  is selected so that  $2 \leq L \leq \frac{T}{2}$ ,  $K$  is related to  $L$  and  $T$  with

$K = T - L + 1$ . The trajectory matrix is then split into two  $K \times (L - 1)$  matrices, as described above. The remaining steps of the DMD algorithm do not change.

## 2.2 Least-squares estimated linear trend and periodicities extrapolation with Vector AutoRegression on residues

This prediction procedure begins with a least-squares fit of a linear trend and periodic components (10) to the input time series (separately for each of variables  $V_i$ ).

$$V_i = A_i + B_i t + \sum_j^k a_{i,j} \sin(\omega_{i,j} t + \phi_{i,j}) + e_i \quad (10)$$

where  $V$  stands for a variable of interest, i.e., UT1-UTC, LOD, or AAM;  $A, B$  are the intercept and slope of a linear trend;  $a, \omega, \phi$  are the amplitude, frequency and phase of a sine wave,  $e$  stands for an error term,  $[A, B, a, \omega, \phi]$  to be determined. Residuals  $V_i^{Res} = \hat{e}_i$  obtained after eliminating the linear trend and periodicities in (10) are subject to a joint prediction through  $p$  - lagged vector autoregressive model LS+VAR. VAR model describes a dynamic dependence between variables, i.e., links current values of variables with their past values, and past values of other variables in the system and may be expressed as:

$$\mathbf{V}_T^{Res} = \mathbf{c} + \mathbf{A}'_p \mathbf{V}_{T-p}^{Res} + \mathbf{A}'_{p-1} \mathbf{V}_{T-p+1}^{Res} + \dots + \mathbf{A}'_1 \mathbf{V}_{T-1}^{Res} + \mathbf{e}_T^{Res} \quad (11)$$

where a constant vector  $\mathbf{c}$  ( $nv \times 1$ ) accounts for a non-zero mean value of the vector process, each of  $\mathbf{V}^{Res}$  ( $nv \times 1$ ) stores residual values of variables at appropriate time delay, each  $\mathbf{A}'$  is a  $nv \times nv$  matrix of coefficients and  $\mathbf{e}^{Res}$  ( $nv \times 1$ ) is a vector of error terms,  $nv$  denotes a number of variables.

After the estimation of coefficients matrices  $\mathbf{A}'$  in (11), the forecast may be performed through the successive use of the formula:

$$\hat{\mathbf{V}}_{T+h}^{Res} = [\hat{\mathbf{A}}'_1 \quad \hat{\mathbf{A}}'_2 \dots \hat{\mathbf{A}}'_p] \begin{bmatrix} \hat{\mathbf{V}}_{T+h-1}^{Res} \\ \hat{\mathbf{V}}_{T+h-2}^{Res} \\ \vdots \\ \hat{\mathbf{V}}_{T+h-p}^{Res} \end{bmatrix} \quad (12)$$

where  $h$  denotes a time-step of forecast horizon and if  $h - i \leq 0$  where  $i = 1, 2, \dots, p$  then  $\hat{\mathbf{V}}_{T+h-i}^{Res} = \mathbf{V}_{T+h-i}^{Res}$ . Finally, the extrapolated trend and periodic components of (10) are combined with the predicted residuals (12).

## 3 Data description and processing details

The short-term (30 days into the future) UT1-UTC and LOD forecast was performed using IERS EOP 14 C04 (IAU2000A) series as a reference (Bizouard et al., 2018). AAM series (Dobslaw and Dill, 2018) was also used – as an auxiliary data source in LS+VAR-based prediction procedure to potentially strengthen the prediction of UT1-UTC and LOD. The prediction experiment was completed in two variants, the first one with the removal of effect of zonal tides (recommended by IERS Conventions (2010) (Petit and Luzum, 2010)) and the other omitting this step.

The first stage in the prediction procedure involved identifying sets of best-performing steering parameters on the yearly period immediately preceding the period of the relevant forecasts (e.g., forecasts within 2018 were based on steering parameters determined for the year 2017). These sets of parameters were selected based on the condition of the least sum of squares of differences between the observed and predicted values for all 30 days of the forecasts.

The searching loop responsible for preselecting sets of parameters involved:

in the case of DMD:

- input time series length ( $T$ ),
- number of snapshots ( $L$ ).

in the case of LS+VAR:

- input time series length ( $T$ ) for estimation of linear trend and periodic components,
- number of periodic components ( $PC$ ),
- subseries of ( $T$ ) for LS+VAR parameters estimation ( $subT$ ),
- autoregression order ( $p$ ).

The sets of parameters selected in this way were then applied in two kinds of prediction approaches: adaptive and averaged. In the adaptive approach, before every single proper 30-day prediction, a preliminary one was performed of the preceding 30 days. This preliminary forecast was made with pre-selected sets of parameters obtained in the aforementioned step, and the method yielding the lowest number of prediction errors was applied to the final current forecast, and the procedure was repeated until the last 30-day forecast was completed. The averaged approach differs from the adaptive one in that the forecasts are made for all sets of pre-selected parameters, and the actual 30-day forecast is computed as the average of these forecasts.

Table 1 presents all variants of prediction methods and data combinations used in this contribution. In the case of LS+VAR, there was a joint forecast of either two (UT1-UTC, LOD; UT1-UTC, AAM; LOD, AAM) or three variables (UT1-UTC, LOD, AAM) but the prediction procedure was optimized so that the one variable of the group was treated as the primary variable and the remaining ones as auxiliary ones. A prediction option without removing the effect of zonal tides is shown in Table 1 with the subscript “nc” (not corrected).

## 4 Results

To measure the quality of predictions using the examined methods and different data combinations the mean absolute prediction error (MAPE) given by (13) was used:

$$MAPE_j = \frac{1}{n} \sum_{i=1}^n |O_{i,j} - P_{i,j}| \quad (13)$$

where:  $n$  is a number of predictions,  $j$  is a prediction day number,  $O$  means *observed* and  $P$  - for *predicted* (here it is either UT1-UTC or LOD).

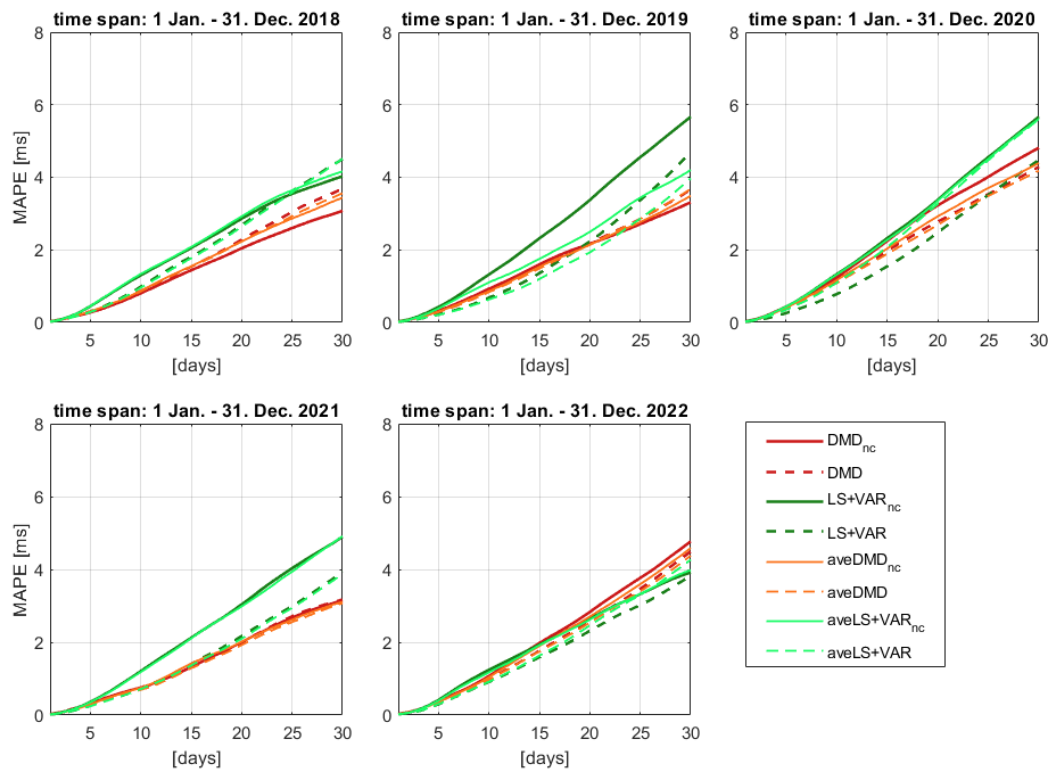
Figures 1 and 2 show MAPEs for a 30-day prediction of UT1-UTC for the yearly time spans 2018–2022 using several methods of forecast - different variations of DMD and LS+VAR. The results show that DMD, in time spans 2018–2021, is characterized by the smallest MAPEs for the 30th day of prediction. In 2022 the most accurate method is LS+VAR in both mass and motion terms using 3 input time series (UT1-UTC, LOD and AAM mass and motion terms). Clearly, for the first day of prediction, MAPEs for all methods are comparable and are at the level of around 0.02 ms. Results of predictions up to 5–7 days into the future indicate that the inclusion of AAM data in the LS+VAR prediction procedure decreases forecast errors only marginally. Interestingly, there is no significant improvement in DMD predictions of UT1-UTC when tidal effects are removed, while the improvement in the LS+VAR forecast is noticeable.

Tables 2 and 3 offers a more detailed presentation of the results of 30-day UT1-UTC predictions for all methods in the yearly time spans 2018–2022 (for selected days of forecast). For the 5th and 10th day of the forecast, the combination of LS+VAR and AAM data (using 3 input time series) achieved the smallest average errors of around 0.29 ms and 0.88 ms, respectively. The longer the range of

**Table 1.** Summary of variants of prediction methods and data combinations

| Acronym                             | Description  |
|-------------------------------------|--|
| DMD, DMD <sub>nc</sub> (*)          | adaptive DMD prediction of UT1-UTC or LOD                                  |
| LS+VAR, LS+VAR <sub>nc</sub>        | adaptive LS+VAR prediction of UT1-UTC and LOD                              |
| aveDMD, aveDMD <sub>nc</sub>        | averaged DMD prediction of UT1-UTC or LOD                                  |
| aveLS+VAR, aveLS+VAR <sub>nc</sub>  | averaged LS+VAR prediction of UT1-UTC and LOD                              |
| LS+VAR_AAM (2)                      | adaptive LS+VAR prediction of UT1-UTC or LOD and AAM mass and motion terms |
| LS+VAR_AAM (3)                      | adaptive LS+VAR prediction of UT1-UTC, LOD and AAM mass and motion terms   |
| LS+VAR_AAM <sub>mass</sub> (2)      | adaptive LS+VAR prediction of UT1-UTC or LOD and AAM mass term             |
| LS+VAR_AAM <sub>mass</sub> (3)      | adaptive LS+VAR prediction of UT1-UTC, LOD and AAM mass term               |
| LS+VAR_AAM <sub>motion</sub> (2)    | adaptive LS+VAR prediction of UT1-UTC or LOD and AAM motion term           |
| LS+VAR_AAM <sub>motion</sub> (3)    | adaptive LS+VAR prediction of UT1-UTC, LOD and AAM motion term             |
| aveLS+VAR_AAM (2)                   | averaged LS+VAR prediction of UT1-UTC or LOD and AAM mass and motion terms |
| aveLS+VAR_AAM (3)                   | averaged LS+VAR prediction of UT1-UTC, LOD and AAM mass and motion terms   |
| aveLS+VAR_AAM <sub>mass</sub> (2)   | averaged LS+VAR prediction of UT1-UTC or LOD and AAM mass term             |
| aveLS+VAR_AAM <sub>mass</sub> (3)   | averaged LS+VAR prediction of UT1-UTC, LOD and AAM mass term               |
| aveLS+VAR_AAM <sub>motion</sub> (2) | averaged LS+VAR prediction of UT1-UTC or LOD and AAM motion term           |
| aveLS+VAR_AAM <sub>motion</sub> (3) | averaged LS+VAR prediction of UT1-UTC, LOD and AAM motion term             |

(\*) subscript “nc” stands for “not corrected”, (2) or (3) stands for a number of variables involved in a prediction procedure incorporating AAM data.

**Figure 1.** MAPEs of 30-day UT1-UTC prediction for the yearly time spans 2018–2022 (nc = not corrected).

the forecast, the more clearly DMD becomes the most accurate forecast method. Finally, average MAPEs on the 30th day of UT1-UTC prediction vary, depending on the method from 3.77 ms for aveDMD to 6.35 ms for aveLS+VAR AAM (2). Interestingly, the accuracy of the forecasts in 2020 dropped in almost all cases, only LS+VAR<sub>nc</sub> and LS+VAR maintained similar forecast error levels as in the other years. In almost half of the cases, there were smaller prediction errors using the averaged approach in UT1-UTC prediction, relative to adaptive approach. Clearly, LS+VAR AAM procedure prediction based on only 2 input time series is characterized by bigger MAPEs than the corresponding procedure with 3 input time series.

Figures 3 and 4 summarise MAPEs for 30-day predictions of LOD for the yearly time spans 2018–2022 using several methods

of forecast: different variations of DMD and LS+VAR. The results indicate that for almost all time spans the most accurate method is DMD (or its variants). The prediction errors for 2022 showed a comparable accuracy of LOD prediction for almost all methods (except LS+VAR<sub>nc</sub>, aveLS+VAR<sub>nc</sub> and aveLS+VAR AAM<sub>mass</sub> (2)). MAPEs for the first day of forecast for all methods are very similar and are around 0.020 ms – 0.030 ms. Similarly to UT1-UTC prediction results, the ultra-short-term (up to 5–7 days into the future) LOD LS+VAR forecast with additional AAM time series is characterized by smaller errors than LS+VAR procedure without AAM time series. On average, the most accurate methods among the methods without additional AAM data for the 30th day are aveDMD<sub>nc</sub> and aveDMD, while among the LS+VAR variants with AAM informa-

tion, it is aveLS+VAR AAM (3). A comparison of the accuracy of LOD prediction options with and without removal of the effect of zonal tides shows that removing tidal effects has significant impact on prediction accuracy using LS+VAR, while there is no significant decrease of MAPEs in DMD.

Tables 4 and 5 present the selected daily values of MAPEs for 30-day LOD prediction for all methods. For days up to the 5th day, the accuracy of prediction for almost all methods is comparable, except LS+VAR<sub>nc</sub>, aveLS+VAR<sub>nc</sub> and aveLS+VAR AAM<sub>mass</sub> (2), whose accuracy is significantly lower. The results indicate that LS+VAR methods with AAM data (based on 3 input time series) for 5th and 10th days for 2019, 2021 and 2022 are among the most accurate methods. Similarly to UT1-UTC prediction, introducing AAM time

series into LS+VAR forecast procedure marginally increases the accuracy for 5–10 day range, relative to LS+VAR predictions without AAM data. After the 10th day the advantage of DMD-based methods is noticeable. On the 20th day of prediction, DMD-based methods reach averaged MAPEs between 0.174 ms and 0.182 ms, while other methods exceed 0.200 ms. For 2018, 2019 and 2022 aveDMD provided the most accurate LOD predictions for the 30th day, whilst in 2020 DMD<sub>nc</sub> and in 2021 DMD reached the smallest values of MAPEs. The results (on average) for the 30th day vary from 0.176 ms (aveDMD<sub>nc</sub> and aveDMD) to 0.242 ms for aveLS+VAR<sub>nc</sub>. Removing tidal effects in LS+VAR prediction procedure decreased the averaged MAPEs for the 30th day of predictions from 0.240 ms to 0.227 ms (LS+VAR) and from 0.242 ms to 0.221 ms (aveLS+VAR). In

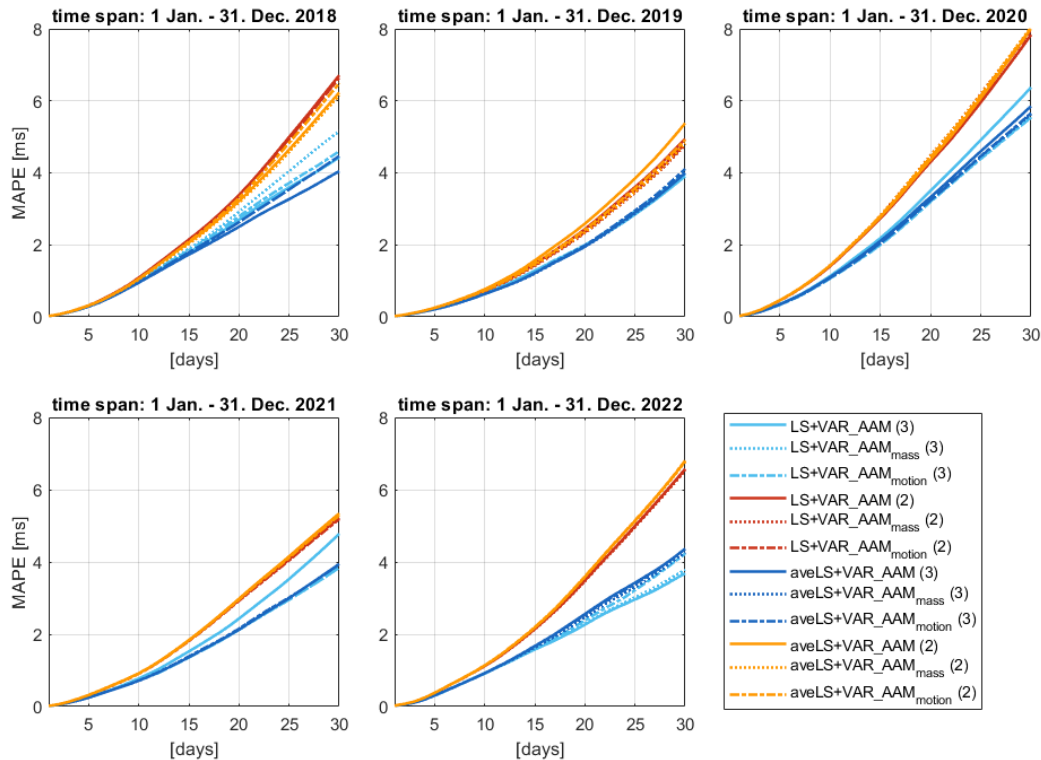


Figure 2. MAPEs of 30-day UT1-UTC prediction with AAM data for the yearly time spans 2018–2022.

Table 2. MAPEs for 30-day UT1-UTC prediction for the yearly time spans 2018–2022 [ms].

| Method                              | Day | 2018        | 2019        | 2020        | 2021        | 2022        | Average     |
|-------------------------------------|-----|-------------|-------------|-------------|-------------|-------------|-------------|
| DMD <sub>nc</sub> / DMD             | 5   | 0.28 / 0.30 | 0.32 / 0.29 | 0.43 / 0.40 | 0.38 / 0.34 | 0.38 / 0.34 | 0.36 / 0.33 |
| LS+VAR <sub>nc</sub> / LS+VAR       |     | 0.45 / 0.30 | 0.41 / 0.21 | 0.43 / 0.25 | 0.41 / 0.30 | 0.41 / 0.30 | 0.42 / 0.27 |
| aveDMD <sub>nc</sub> / aveDMD       |     | 0.30 / 0.29 | 0.30 / 0.29 | 0.40 / 0.39 | 0.29 / 0.29 | 0.36 / 0.35 | 0.33 / 0.32 |
| aveLS+VAR <sub>nc</sub> / aveLS+VAR |     | 0.38 / 0.21 | 0.38 / 0.21 | 0.43 / 0.35 | 0.35 / 0.24 | 0.40 / 0.30 | 0.39 / 0.26 |
| DMD <sub>nc</sub> / DMD             | 10  | 0.81 / 0.87 | 0.93 / 0.85 | 1.23 / 1.13 | 0.75 / 0.72 | 1.07 / 0.99 | 0.96 / 0.91 |
| LS+VAR <sub>nc</sub> / LS+VAR       |     | 1.30 / 0.98 | 1.27 / 0.68 | 1.32 / 0.78 | 1.21 / 0.72 | 1.24 / 0.91 | 1.27 / 0.81 |
| aveDMD <sub>nc</sub> / aveDMD       |     | 0.87 / 0.85 | 0.86 / 0.84 | 1.16 / 1.08 | 0.75 / 0.69 | 1.04 / 0.98 | 0.94 / 0.89 |
| aveLS+VAR <sub>nc</sub> / aveLS+VAR |     | 1.34 / 0.96 | 1.10 / 0.63 | 1.31 / 1.09 | 1.18 / 0.71 | 1.17 / 0.92 | 1.22 / 0.86 |
| DMD <sub>nc</sub> / DMD             | 20  | 2.04 / 2.28 | 2.17 / 2.17 | 3.22 / 2.78 | 2.01 / 2.00 | 2.83 / 2.59 | 2.45 / 2.36 |
| LS+VAR <sub>nc</sub> / LS+VAR       |     | 2.86 / 2.68 | 3.18 / 2.23 | 3.37 / 2.47 | 3.04 / 2.17 | 2.65 / 2.31 | 3.02 / 2.37 |
| aveDMD <sub>nc</sub> / aveDMD       |     | 2.24 / 2.23 | 2.14 / 2.15 | 2.92 / 2.69 | 2.01 / 1.93 | 2.70 / 2.54 | 2.40 / 2.31 |
| aveLS+VAR <sub>nc</sub> / aveLS+VAR |     | 2.92 / 2.64 | 2.50 / 1.93 | 3.35 / 3.27 | 2.98 / 2.10 | 2.62 / 2.46 | 2.87 / 2.48 |
| DMD <sub>nc</sub> / DMD             | 30  | 3.08 / 3.69 | 3.31 / 3.66 | 4.81 / 4.29 | 3.15 / 3.17 | 4.77 / 4.49 | 3.82 / 3.86 |
| LS+VAR <sub>nc</sub> / LS+VAR       |     | 4.03 / 4.50 | 5.64 / 4.69 | 5.67 / 4.48 | 4.90 / 3.93 | 3.92 / 3.83 | 4.83 / 4.29 |
| aveDMD <sub>nc</sub> / aveDMD       |     | 3.44 / 3.56 | 3.49 / 3.68 | 4.39 / 4.18 | 3.11 / 3.07 | 4.59 / 4.38 | 3.80 / 3.77 |
| aveLS+VAR <sub>nc</sub> / aveLS+VAR |     | 4.16 / 4.51 | 4.20 / 3.97 | 5.61 / 5.60 | 4.91 / 3.87 | 3.98 / 4.26 | 4.57 / 4.44 |

**Table 3.** MAPEs for 30-day UT1-UTC prediction with AAM data for the yearly time spans 2018–2022 [ms].

| Method  | Day | 2018        | 2019        | 2020        | 2021        | 2022        | Average     |
|---|-----|-------------|-------------|-------------|-------------|-------------|-------------|
| LS+VAR_AAM (3)/<br>LS+VAR_AAM (2)   |     | 0.29 / 0.32 | 0.21 / 0.25 | 0.35 / 0.46 | 0.30 / 0.32 | 0.30 / 0.38 | 0.29 / 0.34 |
| LS+VAR_AAM <sub>mass</sub> (3)/<br>LS+VAR_AAM <sub>mass</sub> (2)           |     | 0.30 / 0.31 | 0.22 / 0.24 | 0.34 / 0.45 | 0.31 / 0.32 | 0.31 / 0.38 | 0.30 / 0.34 |
| LS+VAR_AAM <sub>motion</sub> (3)/<br>LS+VAR_AAM <sub>motion</sub> (2)       | 5   | 0.30 / 0.31 | 0.21 / 0.25 | 0.33 / 0.45 | 0.31 / 0.31 | 0.31 / 0.38 | 0.29 / 0.34 |
| aveLS+VAR_AAM (3)/<br>aveLS+VAR_AAM (2)                                     |     | 0.29 / 0.32 | 0.21 / 0.25 | 0.35 / 0.46 | 0.25 / 0.32 | 0.31 / 0.38 | 0.28 / 0.35 |
| aveLS+VAR_AAM <sub>mass</sub> (3)/<br>aveLS+VAR_AAM <sub>mass</sub> (2)     |     | 0.29 / 0.31 | 0.21 / 0.25 | 0.34 / 0.45 | 0.25 / 0.32 | 0.30 / 0.38 | 0.28 / 0.34 |
| aveLS+VAR_AAM <sub>motion</sub> (3)/<br>aveLS+VAR_AAM <sub>motion</sub> (2) |     | 0.29 / 0.31 | 0.21 / 0.25 | 0.34 / 0.45 | 0.25 / 0.32 | 0.31 / 0.38 | 0.28 / 0.34 |
| LS+VAR_AAM (3)/<br>LS+VAR_AAM (2)   |     | 0.97 / 1.09 | 0.67 / 0.74 | 1.13 / 1.40 | 0.78 / 0.92 | 0.91 / 1.12 | 0.89 / 1.05 |
| LS+VAR_AAM <sub>mass</sub> (3)/<br>LS+VAR_AAM <sub>mass</sub> (2)           |     | 1.02 / 1.07 | 0.67 / 0.72 | 1.07 / 1.43 | 0.72 / 0.92 | 0.92 / 1.12 | 0.88 / 1.05 |
| LS+VAR_AAM <sub>motion</sub> (3)/<br>LS+VAR_AAM <sub>motion</sub> (2)       | 10  | 1.00 / 1.07 | 0.67 / 0.73 | 1.06 / 1.40 | 0.72 / 0.91 | 0.93 / 1.13 | 0.88 / 1.05 |
| aveLS+VAR_AAM (3)/<br>aveLS+VAR_AAM (2)                                     |     | 0.95 / 1.06 | 0.64 / 0.77 | 1.10 / 1.42 | 0.71 / 0.92 | 0.92 / 1.14 | 0.87 / 1.06 |
| aveLS+VAR_AAM <sub>mass</sub> (3)/<br>aveLS+VAR_AAM <sub>mass</sub> (2)     |     | 0.97 / 1.04 | 0.64 / 0.73 | 1.08 / 1.43 | 0.71 / 0.92 | 0.92 / 1.13 | 0.86 / 1.05 |
| aveLS+VAR_AAM <sub>motion</sub> (3)/<br>aveLS+VAR_AAM <sub>motion</sub> (2) |     | 0.97 / 1.06 | 0.64 / 0.74 | 1.08 / 1.42 | 0.72 / 0.91 | 0.92 / 1.14 | 0.87 / 1.05 |
| LS+VAR_AAM (3)/<br>LS+VAR_AAM (2)   |     | 2.70 / 3.39 | 1.98 / 2.44 | 3.50 / 4.30 | 2.43 / 2.95 | 2.27 / 3.49 | 2.58 / 3.31 |
| LS+VAR_AAM <sub>mass</sub> (3)/<br>LS+VAR_AAM <sub>mass</sub> (2)           |     | 2.92 / 3.35 | 2.00 / 2.33 | 3.21 / 4.48 | 2.12 / 2.95 | 2.29 / 3.47 | 2.51 / 3.32 |
| LS+VAR_AAM <sub>motion</sub> (3)/<br>LS+VAR_AAM <sub>motion</sub> (2)       | 20  | 2.79 / 3.36 | 2.00 / 2.36 | 3.19 / 4.41 | 2.12 / 2.93 | 2.38 / 3.49 | 2.50 / 3.31 |
| aveLS+VAR_AAM (3)/<br>aveLS+VAR_AAM (2)                                     |     | 2.50 / 3.22 | 1.95 / 2.59 | 3.32 / 4.37 | 2.13 / 2.98 | 2.56 / 3.59 | 2.49 / 3.35 |
| aveLS+VAR_AAM <sub>mass</sub> (3)/<br>aveLS+VAR_AAM <sub>mass</sub> (2)     |     | 2.63 / 3.18 | 1.95 / 2.35 | 3.24 / 4.48 | 2.13 / 2.98 | 2.46 / 3.58 | 2.48 / 3.31 |
| aveLS+VAR_AAM <sub>motion</sub> (3)/<br>aveLS+VAR_AAM <sub>motion</sub> (2) |     | 2.63 / 3.30 | 1.98 / 2.42 | 3.24 / 4.44 | 2.15 / 2.96 | 2.54 / 3.60 | 2.51 / 3.34 |
| LS+VAR_AAM (3)/<br>LS+VAR_AAM (2)   |     | 4.43 / 6.71 | 3.91 / 4.94 | 6.38 / 7.84 | 4.78 / 5.22 | 3.68 / 6.57 | 4.64 / 6.26 |
| LS+VAR_AAM <sub>mass</sub> (3)/<br>LS+VAR_AAM <sub>mass</sub> (2)           |     | 5.15 / 6.65 | 4.01 / 4.77 | 5.55 / 8.03 | 3.84 / 5.22 | 3.79 / 6.53 | 4.47 / 6.24 |
| LS+VAR_AAM <sub>motion</sub> (3)/<br>LS+VAR_AAM <sub>motion</sub> (2)       | 30  | 4.60 / 6.64 | 3.96 / 4.81 | 5.53 / 7.96 | 3.84 / 5.19 | 4.23 / 6.57 | 4.43 / 6.23 |
| aveLS+VAR_AAM (3)/<br>aveLS+VAR_AAM (2)                                     |     | 4.04 / 6.23 | 4.00 / 5.38 | 5.85 / 8.01 | 3.94 / 5.34 | 4.36 / 6.79 | 4.44 / 6.35 |
| aveLS+VAR_AAM <sub>mass</sub> (3)/<br>aveLS+VAR_AAM <sub>mass</sub> (2)     |     | 4.47 / 6.15 | 3.99 / 4.82 | 5.63 / 8.05 | 3.94 / 5.32 | 4.26 / 6.77 | 4.46 / 6.22 |
| aveLS+VAR_AAM <sub>motion</sub> (3)/<br>aveLS+VAR_AAM <sub>motion</sub> (2) |     | 4.47 / 6.49 | 4.11 / 4.92 | 5.66 / 8.02 | 3.93 / 5.29 | 4.35 / 6.80 | 4.50 / 6.30 |

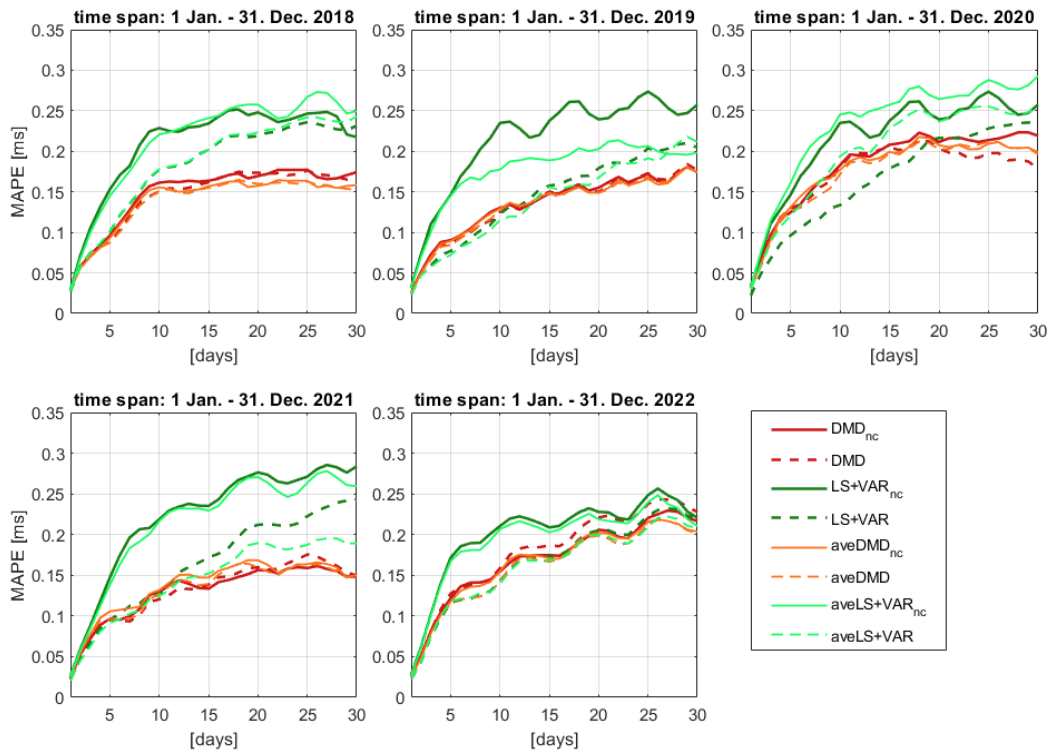


Figure 3. MAPEs of 30-day LOD prediction for the yearly time spans 2018–2022 (nc = not corrected).

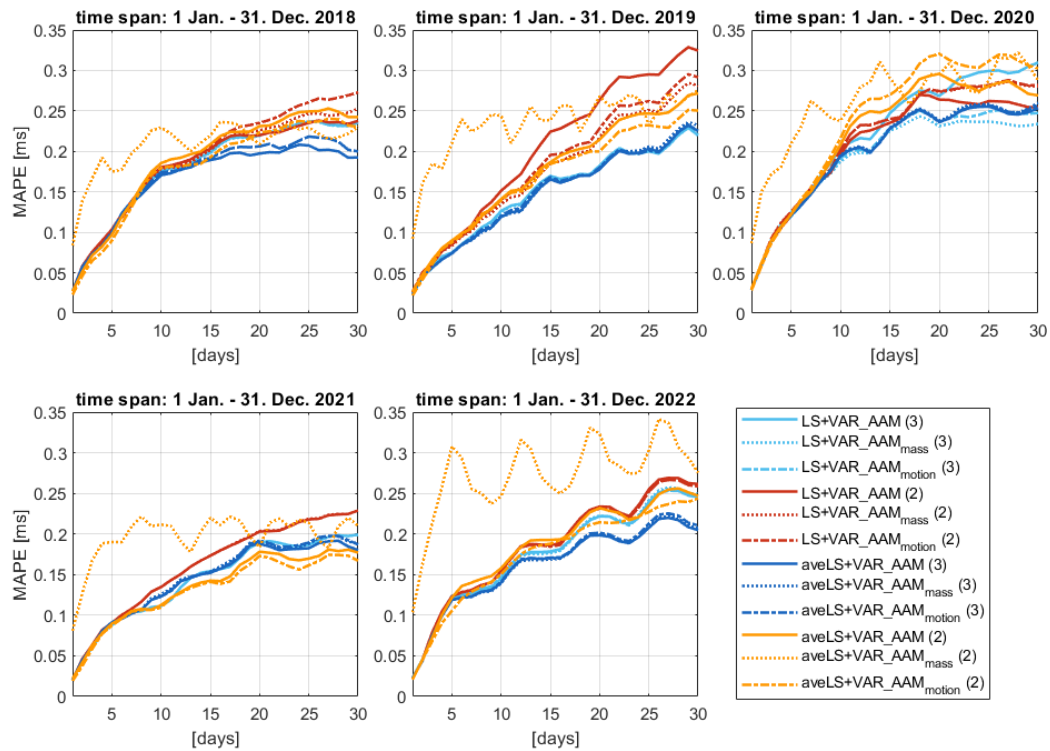


Figure 4. MAPEs of 30-day LOD prediction with AAM data for the yearly time spans 2018–2022.

the case of DMD there were no significant improvements in prediction accuracy after removing tidal effects as compared with the DMD procedure without such a removal. Results indicated a slight decrease of MAPEs in around half of the forecasts using the averaged approach in LOD prediction as compared with the adaptive approach.

## 5 Conclusions

This contribution applied Dynamic Mode Decomposition and a combination of least-squares and vector autoregressive models for UT1-UTC and LOD forecast. Prediction accuracy is presented for five yearly time spans from 2018 to 2022. Prediction procedures involved adaptive and averaged modes differing by the use of sets of steering parameters identified at the preliminary stage of fore-

**Table 4.** MAPEs for 30-day LOD prediction for the yearly time spans 2018–2022 [ms].

| Method                              | Day | 2018          | 2019          | 2020          | 2021          | 2022          | Average       |
|-------------------------------------|-----|---------------|---------------|---------------|---------------|---------------|---------------|
| DMD <sub>nc</sub> / DMD             | 5   | 0.096 / 0.088 | 0.090 / 0.086 | 0.125 / 0.130 | 0.097 / 0.096 | 0.122 / 0.127 | 0.106 / 0.105 |
| LS+VAR <sub>nc</sub> / LS+VAR       |     | 0.153 / 0.101 | 0.167 / 0.077 | 0.146 / 0.096 | 0.148 / 0.095 | 0.172 / 0.116 | 0.157 / 0.097 |
| aveDMD <sub>nc</sub> / aveDMD       |     | 0.093 / 0.088 | 0.089 / 0.084 | 0.131 / 0.127 | 0.106 / 0.097 | 0.118 / 0.115 | 0.107 / 0.102 |
| aveLS+VAR <sub>nc</sub> / aveLS+VAR |     | 0.145 / 0.101 | 0.145 / 0.072 | 0.161 / 0.121 | 0.139 / 0.091 | 0.167 / 0.119 | 0.151 / 0.101 |
| DMD <sub>nc</sub> / DMD             | 10  | 0.161 / 0.151 | 0.130 / 0.125 | 0.183 / 0.181 | 0.130 / 0.120 | 0.155 / 0.159 | 0.152 / 0.147 |
| LS+VAR <sub>nc</sub> / LS+VAR       |     | 0.229 / 0.178 | 0.197 / 0.123 | 0.235 / 0.134 | 0.219 / 0.127 | 0.210 / 0.143 | 0.218 / 0.141 |
| aveDMD <sub>nc</sub> / aveDMD       |     | 0.156 / 0.151 | 0.129 / 0.127 | 0.177 / 0.172 | 0.132 / 0.127 | 0.155 / 0.142 | 0.150 / 0.144 |
| aveLS+VAR <sub>nc</sub> / aveLS+VAR |     | 0.221 / 0.178 | 0.177 / 0.115 | 0.245 / 0.194 | 0.217 / 0.125 | 0.207 / 0.139 | 0.213 / 0.150 |
| DMD <sub>nc</sub> / DMD             | 20  | 0.170 / 0.174 | 0.155 / 0.150 | 0.212 / 0.203 | 0.156 / 0.160 | 0.206 / 0.221 | 0.180 / 0.182 |
| LS+VAR <sub>nc</sub> / LS+VAR       |     | 0.248 / 0.219 | 0.204 / 0.179 | 0.239 / 0.217 | 0.276 / 0.212 | 0.228 / 0.205 | 0.239 / 0.206 |
| aveDMD <sub>nc</sub> / aveDMD       |     | 0.158 / 0.160 | 0.149 / 0.149 | 0.208 / 0.203 | 0.168 / 0.160 | 0.202 / 0.199 | 0.177 / 0.174 |
| aveLS+VAR <sub>nc</sub> / aveLS+VAR |     | 0.258 / 0.223 | 0.203 / 0.168 | 0.264 / 0.237 | 0.271 / 0.190 | 0.219 / 0.199 | 0.243 / 0.203 |
| DMD <sub>nc</sub> / DMD             | 30  | 0.174 / 0.164 | 0.174 / 0.177 | 0.219 / 0.178 | 0.148 / 0.150 | 0.217 / 0.228 | 0.186 / 0.179 |
| LS+VAR <sub>nc</sub> / LS+VAR       |     | 0.217 / 0.231 | 0.219 / 0.204 | 0.257 / 0.236 | 0.284 / 0.243 | 0.221 / 0.219 | 0.240 / 0.227 |
| aveDMD <sub>nc</sub> / aveDMD       |     | 0.158 / 0.153 | 0.174 / 0.174 | 0.196 / 0.199 | 0.150 / 0.151 | 0.204 / 0.202 | 0.176 / 0.176 |
| aveLS+VAR <sub>nc</sub> / aveLS+VAR |     | 0.250 / 0.243 | 0.198 / 0.211 | 0.293 / 0.253 | 0.259 / 0.189 | 0.210 / 0.208 | 0.242 / 0.221 |

cast. In addition, external data, Atmospheric Angular Momentum were included in the LS+VAR-based prediction procedure. Predictions were also performed with and without corrections due to tidal effects.

Results indicate that there is no single most accurate variant for all 30 days UT1–UTC predictions. For years 2018, 2019 and 2021 DMD<sub>nc</sub> offered the lowest values of MAPEs, whilst for 2020 aveDMD and in 2022 LS+VAR AAM (3) obtained the highest accuracy. The results show that aveDMD is the most accurate method in almost all time periods for the 30th day of LOD prediction with the MAPE in the range of 0.158 – 0.204 ms.

Interestingly, the inclusion of AAM time series in the LS+VAR prediction procedure did not visibly increase the accuracy of the UT1–UTC or LOD forecasts. The results showed that incorporating AAM data into the LS+VAR prediction (comparing all variants of LS+VAR AAM and aveLS+VAR AAM with corresponding LS+VAR and aveLS+VAR) improved the UT1–UTC prediction accuracy in only 20 out of 120 cases and – in the case of LOD – in 26 out of 120 cases. The increase in prediction accuracy, if it occurs, in the case of UT1–UTC is the most evident for the 30th day of prediction and in the case of LOD – for ultra short-term forecast (up to 5 – 10 days).

In more than half of the cases, there was a slight improvement in UT1–UTC and LOD forecasts using the averaged approach comparing to the adaptive one. The results indicate that averaged approach, and not the adaptive one (for DMD and LS+VAR predictions together), improves UT1–UTC predictions (in 54 out of 80 cases) marginally more often than LOD predictions (in 47 out of 80 cases). It can be also noticed that the averaged approach, compared to the adaptive approach, improves DMD prediction 53 times (of UT1–UTC and LOD predictions together), while LS+VAR prediction – 48 times. In the case of UT1–UTC LS+VAR AAM prediction, in both approaches (using 2 and 3 input time series), there was no improvement using the averaged approach comparing to the adaptive approach. On the other hand, in LOD predictions when 2 input time series were involved in a LS+VAR prediction procedure there were reductions in forecast errors (in favour of the averaged approach over the adaptive approach) only in 18 out of 75 cases, while when using 3 input time series these reductions occurred in 11 out of 75 cases.

The results also indicate that the use of 3 variables (UT1–UTC, LOD and AAM component) in LS+VAR AAM prediction procedure is characterized by lower numbers of prediction errors than using only 2 variables (UT1–UTC/LOD and AAM component). The prediction accuracy of all variants of LS+VAR AAM (3) procedure rather than

the corresponding variants of LS+VAR AAM (2), in case of UT1–UTC, increased in all cases with an average improvement of around 20.9% and in the case of LOD – in 106 out of 120 cases with improvement of around 13.8%. It can therefore be concluded that, in these cases, including an additional correlated variable in the LS+VAR prediction procedure significantly improves the accuracy of the forecast.

There was a marginal decrease of MAPEs in DMD-based predictions of UT1–UTC and LOD when tidal effects were removed comparing to the procedures without removing these effects, whilst it is much clearer in the LS+VAR-based forecast. These improvements in the 30th day of DMD and LS+VAR predictions of UT1–UTC vary from 0.04 ms to 0.52 ms and from 0.01 ms to 1.19 ms, respectively. The corresponding values for the LOD forecast are in range from 0.002 ms to 0.041 ms (in the case of DMD) and from 0.002 ms to 0.070 ms (in the case of LS+VAR).

A potential explanation for the greater impact of removing (or not removing) tidal oscillations on the LS+VAR-based forecast than on the DMD is that LS+VAR is based on the traditional approach of first removing the trend and periodic components and then applying a VAR model to the residuals. In the procedure without removing the tidal oscillations, they remain as the residuals and therefore directly affect the forecast results. DMD, on the other hand, is a data-driven method which does not rely on any prior assumptions beyond the inherent dynamics observed over time. DMD was designed to search for patterns in trends and frequencies, and their evolution in time, hence, it is very likely that it identified some of the tidal frequencies, and the remaining ones were replaced with some artificial frequencies found in the series on which the DMD model was built.

It is also worth noting that the accuracy of both UT1–UTC and LOD predictions for 2020 and 2022 decreased in almost all cases. The large values of MAPE may be caused by, among other things, such phenomena as El Niño and La Niña occurring at the same time (Xu et al. 2022a; [https://origin.cpc.ncep.noaa.gov/products/analysis\\_monitoring/ensostuff/ONI\\_v5.php](https://origin.cpc.ncep.noaa.gov/products/analysis_monitoring/ensostuff/ONI_v5.php)).

**Table 5.** MAPEs for 30-day LOD prediction with AAM data for the yearly time spans 2018–2022 [ms].

| Method  | Day | 2018          | 2019          | 2020          | 2021          | 2022          | Average       |
|---|-----|---------------|---------------|---------------|---------------|---------------|---------------|
| LS+VAR_AAM (3)/<br>LS+VAR_AAM (2)   | 5   | 0.100 / 0.104 | 0.075 / 0.086 | 0.125 / 0.120 | 0.088 / 0.091 | 0.122 / 0.123 | 0.102 / 0.105 |
| LS+VAR_AAM <sub>mass</sub> (3)/<br>LS+VAR_AAM <sub>mass</sub> (2)           |     | 0.100 / 0.101 | 0.075 / 0.083 | 0.120 / 0.125 | 0.088 / 0.090 | 0.123 / 0.123 | 0.101 / 0.104 |
| LS+VAR_AAM <sub>motion</sub> (3)/<br>LS+VAR_AAM <sub>motion</sub> (2)       |     | 0.100 / 0.101 | 0.075 / 0.085 | 0.120 / 0.125 | 0.088 / 0.091 | 0.124 / 0.123 | 0.101 / 0.105 |
| aveLS+VAR_AAM (3)/<br>aveLS+VAR_AAM (2)                                     |     | 0.099 / 0.097 | 0.074 / 0.090 | 0.121 / 0.122 | 0.091 / 0.090 | 0.119 / 0.122 | 0.101 / 0.104 |
| aveLS+VAR_AAM <sub>mass</sub> (3)/<br>aveLS+VAR_AAM <sub>mass</sub> (2)     |     | 0.101 / 0.175 | 0.074 / 0.210 | 0.121 / 0.209 | 0.092 / 0.190 | 0.119 / 0.308 | 0.101 / 0.219 |
| aveLS+VAR_AAM <sub>motion</sub> (3)/<br>aveLS+VAR_AAM <sub>motion</sub> (2) |     | 0.101 / 0.090 | 0.074 / 0.088 | 0.121 / 0.123 | 0.091 / 0.087 | 0.119 / 0.105 | 0.101 / 0.099 |
| LS+VAR_AAM (3)/<br>LS+VAR_AAM (2)   | 10  | 0.176 / 0.181 | 0.126 / 0.151 | 0.205 / 0.196 | 0.110 / 0.135 | 0.144 / 0.154 | 0.152 / 0.163 |
| LS+VAR_AAM <sub>mass</sub> (3)/<br>LS+VAR_AAM <sub>mass</sub> (2)           |     | 0.175 / 0.179 | 0.125 / 0.135 | 0.187 / 0.201 | 0.111 / 0.135 | 0.145 / 0.154 | 0.149 / 0.161 |
| LS+VAR_AAM <sub>motion</sub> (3)/<br>LS+VAR_AAM <sub>motion</sub> (2)       |     | 0.176 / 0.180 | 0.126 / 0.140 | 0.191 / 0.201 | 0.112 / 0.135 | 0.147 / 0.154 | 0.150 / 0.162 |
| aveLS+VAR_AAM (3)/<br>aveLS+VAR_AAM (2)                                     |     | 0.171 / 0.185 | 0.119 / 0.141 | 0.194 / 0.208 | 0.124 / 0.113 | 0.140 / 0.158 | 0.149 / 0.161 |
| aveLS+VAR_AAM <sub>mass</sub> (3)/<br>aveLS+VAR_AAM <sub>mass</sub> (2)     |     | 0.174 / 0.229 | 0.119 / 0.244 | 0.195 / 0.238 | 0.126 / 0.212 | 0.139 / 0.247 | 0.151 / 0.234 |
| aveLS+VAR_AAM <sub>motion</sub> (3)/<br>aveLS+VAR_AAM <sub>motion</sub> (2) |     | 0.174 / 0.180 | 0.121 / 0.139 | 0.195 / 0.216 | 0.123 / 0.110 | 0.141 / 0.150 | 0.151 / 0.159 |
| LS+VAR_AAM (3)/<br>LS+VAR_AAM (2)   | 20  | 0.221 / 0.220 | 0.181 / 0.263 | 0.269 / 0.264 | 0.190 / 0.203 | 0.224 / 0.234 | 0.217 / 0.237 |
| LS+VAR_AAM <sub>mass</sub> (3)/<br>LS+VAR_AAM <sub>mass</sub> (2)           |     | 0.219 / 0.226 | 0.180 / 0.217 | 0.231 / 0.274 | 0.189 / 0.204 | 0.221 / 0.231 | 0.208 / 0.230 |
| LS+VAR_AAM <sub>motion</sub> (3)/<br>LS+VAR_AAM <sub>motion</sub> (2)       |     | 0.220 / 0.235 | 0.182 / 0.228 | 0.237 / 0.274 | 0.190 / 0.203 | 0.222 / 0.231 | 0.210 / 0.234 |
| aveLS+VAR_AAM (3)/<br>aveLS+VAR_AAM (2)                                     |     | 0.197 / 0.231 | 0.178 / 0.215 | 0.237 / 0.296 | 0.188 / 0.178 | 0.198 / 0.232 | 0.200 / 0.230 |
| aveLS+VAR_AAM <sub>mass</sub> (3)/<br>aveLS+VAR_AAM <sub>mass</sub> (2)     |     | 0.206 / 0.209 | 0.179 / 0.268 | 0.238 / 0.295 | 0.192 / 0.184 | 0.199 / 0.323 | 0.203 / 0.256 |
| aveLS+VAR_AAM <sub>motion</sub> (3)/<br>aveLS+VAR_AAM <sub>motion</sub> (2) |     | 0.206 / 0.224 | 0.180 / 0.200 | 0.236 / 0.321 | 0.191 / 0.173 | 0.201 / 0.214 | 0.203 / 0.226 |
| LS+VAR_AAM (3)/<br>LS+VAR_AAM (2)   | 30  | 0.235 / 0.238 | 0.220 / 0.325 | 0.310 / 0.255 | 0.199 / 0.229 | 0.246 / 0.261 | 0.242 / 0.261 |
| LS+VAR_AAM <sub>mass</sub> (3)/<br>LS+VAR_AAM <sub>mass</sub> (2)           |     | 0.233 / 0.253 | 0.221 / 0.281 | 0.234 / 0.280 | 0.197 / 0.229 | 0.249 / 0.259 | 0.227 / 0.260 |
| LS+VAR_AAM <sub>motion</sub> (3)/<br>LS+VAR_AAM <sub>motion</sub> (2)       |     | 0.234 / 0.273 | 0.220 / 0.292 | 0.247 / 0.282 | 0.199 / 0.229 | 0.246 / 0.259 | 0.229 / 0.267 |
| aveLS+VAR_AAM (3)/<br>aveLS+VAR_AAM (2)                                     |     | 0.193 / 0.242 | 0.225 / 0.272 | 0.253 / 0.269 | 0.180 / 0.177 | 0.205 / 0.247 | 0.211 / 0.241 |
| aveLS+VAR_AAM <sub>mass</sub> (3)/<br>aveLS+VAR_AAM <sub>mass</sub> (2)     |     | 0.200 / 0.230 | 0.232 / 0.276 | 0.260 / 0.287 | 0.188 / 0.210 | 0.208 / 0.276 | 0.218 / 0.256 |
| aveLS+VAR_AAM <sub>motion</sub> (3)/<br>aveLS+VAR_AAM <sub>motion</sub> (2) |     | 0.200 / 0.230 | 0.225 / 0.250 | 0.257 / 0.302 | 0.187 / 0.167 | 0.210 / 0.244 | 0.216 / 0.239 |

### Acknowledgements

Research project supported by program „Excellence initiative – research university” for the AGH University of Krakow.

The paper is a result of research on geospatial methods carried out within the statutory research grant no. 16.16.150.545 at the Department of Integrated Geodesy and Cartography, AGH University of Krakow.

We gratefully acknowledge Poland’s high-performance com-

puting infrastructure PLGrid (HPC Centers: ACK Cyfronet AGH) for providing computer facilities and support within computational grant Nos. PLG/2022/015968 and PLG/2023/016281.

Intermediate results are available on the website accompanying this article: [home.agh.edu.pl/mmichalc](http://home.agh.edu.pl/mmichalc).

## References

- Bizouard, C., Lambert, S., Gattano, C., Becker, O., and Richard, J.-Y. (2018). The IERS EOP 14C04 solution for earth orientation parameters consistent with ITRF 2014. *Journal of Geodesy*, 93(5):621–633, doi:10.1007/s00190-018-1186-3.
- Dick, W. R. and Thaller, D. (2020). IERS Annual Report 2018. Technical report, International Earth Rotation and Reference Systems Service, Central Bureau.
- Dill, R., Dobsław, H., and Thomas, M. (2018). Improved 90-day Earth orientation predictions from angular momentum forecasts of atmosphere, ocean, and terrestrial hydrosphere. *Journal of Geodesy*, 93(3):287–295, doi:10.1007/s00190-018-1158-7.
- Dobsław, H. and Dill, R. (2018). Predicting Earth orientation changes from global forecasts of atmosphere-hydrosphere dynamics. *Advances in Space Research*, 61(4):1047–1054, doi:10.1016/j.asr.2017.11.044.
- Gambis, D. and Luzum, B. (2011). Earth rotation monitoring, UT1 determination and prediction. *Metrologia*, 48(4):S165–S170, doi:10.1088/0026-1394/48/4/S06.
- Gross, R. S., Eubanks, T., Steppe, J., Freedman, A., Dickey, J., and Runge, T. (1998). A Kalman-filter-based approach to combining independent Earth-orientation series. *Journal of Geodesy*, 72:215–235, doi:10.1007/s001900050162.
- Gross, R. S., Fukumori, I., Menemenlis, D., and Gegout, P. (2004). Atmospheric and oceanic excitation of length-of-day variations during 1980–2000. *Journal of Geophysical Research: Solid Earth*, 109(B1), doi:10.1029/2003jb002432.
- Guessoum, S., Belda, S., Ferrándiz, J. M., Modiri, S., Raut, S., Dhar, S., Heinkelmann, R., and Schuh, H. (2022). The short-term prediction of Length of Day using 1D convolutional neural networks (1D CNN). *Sensors*, 22(23):9517, doi:10.3390/s22239517.
- Holton, J. R. and Dmowska, R. (1989). *El Niño, La Niña, and the southern oscillation*. Academic press, Cambridge, MA, USA.
- Höpfner, J. (1998). Seasonal variations in length of day and atmospheric angular momentum. *Geophysical Journal International*, 135(2):407–437, doi:10.1046/j.1365-246X.1998.00648.x.
- Kalarus, M., Schuh, H., Kosek, W., Akyilmaz, O., Bizouard, C., Gambis, D., Gross, R., Jovanović, B., Kumakshev, S., Kutterer, H., Mendes Cerveira, P. J., Pasynok, S., and Zotov, L. (2010). Achievements of the Earth orientation parameters prediction comparison campaign. *Journal of Geodesy*, 84(10):587–596, doi:10.1007/s00190-010-0387-1.
- Kiani Shahvandi, M., Schartner, M., and Soja, B. (2022). Neural ODE differential learning and its application in polar motion prediction. *Journal of Geophysical Research: Solid Earth*, 127(11), doi:10.1029/2022jb024775.
- Kur, T., Dobsław, H., Śliwińska, J., Nastula, J., Wińska, M., and Partyka, A. (2022). Evaluation of selected short-term predictions of UT1-UTC and LOD collected in the second earth orientation parameters prediction comparison campaign. *Earth, Planets and Space*, 74(1), doi:10.1186/s40623-022-01753-9.
- Lei, Y., Cai, H., and Zhao, D. (2017). Improvement of the prediction accuracy of polar motion using empirical mode decomposition. *Geodesy and Geodynamics*, 8(2):141–146, doi:10.1016/j.geog.2016.09.007.
- Liao, D., Wang, Q., Zhou, Y., Liao, X., and Huang, C. (2012). Long-term prediction of the Earth Orientation Parameters by the artificial neural network technique. *Journal of Geodynamics*, 62:87–92, doi:10.1016/j.jog.2011.12.004.
- Michalczak, M. and Ligas, M. (2021). Kriging-based prediction of the Earth's pole coordinates. *Journal of Applied Geodesy*, 15(3):233–241, doi:10.1515/jag-2021-0007.
- Michalczak, M. and Ligas, M. (2022). The (ultra) short term prediction of length-of-day using kriging. *Advances in Space Research*, 70(3):610–620, doi:10.1016/j.asr.2022.05.007.
- Modiri, S., Belda, S., Hoseini, M., Heinkelmann, R., Ferrándiz, J. M., and Schuh, H. (2020). A new hybrid method to improve the ultra-short-term prediction of LOD. *Journal of Geodesy*, 94(2), doi:10.1007/s00190-020-01354-y.
- Nastula, J., Chin, T. M., Gross, R., Śliwińska, J., and Wińska, M. (2020). Smoothing and predicting celestial pole offsets using a Kalman filter and smoother. *Journal of Geodesy*, 94(3), doi:10.1007/s00190-020-01349-9.
- Niedzielski, T. and Kosek, W. (2011). *Prediction Analysis of UT1-UTC Time Series by Combination of the Least-Squares and Multivariate Autoregressive Method*, pages 153–157. Springer Berlin Heidelberg, doi:10.1007/978-3-642-22078-4\_23.
- Okhotnikov, G. and Golyandina, N. (2019). EOP time series prediction using singular spectrum analysis. In Corpetti, T., Ienco, D., and Interdonato, R., editors, *Proceedings of MACLEAN: MACHINE learning for Earth observation workshop, RWTH Aachen University, CEUR Workshop Proceedings*.
- Petit, G. and Luzum, B. (2010). Iers conventions. Technical report, IERS Technical Note 36, Verlag des Bundesamts für Kartographie und Geodäsie Frankfurt am Main, Germany.
- Schmid, P. J. (2010). Dynamic mode decomposition of numerical and experimental data. *Journal of Fluid Mechanics*, 656:5–28, doi:10.1017/S0022112010001217.
- Schuh, H., Ulrich, M., Egger, D., Müller, J., and Schwegmann, W. (2002). Prediction of Earth orientation parameters by artificial neural networks. *Journal of Geodesy*, 76(5):247–258, doi:10.1007/s00190-001-0242-5.
- Soffel, M. (2013). *Space-Time Reference Systems*. SpringerLink. Springer, Berlin. Description based upon print version of record.
- Tirunagari, S., Kouchaki, S., Poh, N., Bober, M., and Windridge, D. (2017). Dynamic mode decomposition for univariate time series: analysing trends and forecasting. *hal-01463744f*.
- Tu, J. H., Rowley, W. C., Luchtenburg, D. M., Brunton, S. L., and Kutz, J. N. (2014). On dynamic mode decomposition: Theory and applications. *Journal of Computational Dynamics*, 1(2):391–421, doi:10.3934/jcd.2014.1.391.
- Xu, X., Zhou, Y., and Liao, X. (2012). Short-term earth orientation parameters predictions by combination of the least-squares, AR model and Kalman filter. *Journal of Geodynamics*, 62:83–86, doi:10.1016/j.jog.2011.12.001.
- Xu, X., Zhou, Y., and XU, C. (2022a). Earth rotation parameters prediction and climate change indicators in it. *Artificial Satellites*, 57(s1):262–273, doi:10.2478/arsa-2022-0023.
- Xu, X.-Q., Zhou, Y.-H., Duan, P.-S., Fang, M., Kong, Z.-Y., Xu, C.-C., and An, X.-R. (2022b). Contributions of oceanic and continental AAM to interannual variation in  $\Delta$ LOD with the detection of 2020–2021 La Nina event. *Journal of Geodesy*, 96(6), doi:10.1007/s00190-022-01632-x.
- Śliwińska, J., Kur, T., Wińska, M., Nastula, J., Dobsław, H., and Partyka, A. (2022). Second Earth Orientation Parameters prediction comparison campaign (2nd EOP PCC): Overview. *Artificial Satellites*, 57(s1):237–253, doi:10.2478/arsa-2022-0021.